FEBS 26802 FEBS Letters 532 (2002) 333–337

A directional electron transfer regulator based on heme-chain architecture in the small tetraheme cytochrome *c* from *Shewanella oneidensis*

Erisa Harada[a,b,c], Jiro Kumagai[b], Kiyoshi Ozawa[b], Shinichiro Imabayashi[b], Alexandre S. Tsapin[d], Kenneth H. Nealson[d], Terrance E. Meyer[e], Michael A. Cusanovich[e], Hideo Akutsu[a,f,*]

[a] *Institute for Protein Research, Osaka University, Yamadaoka, Suita, Osaka 565-0871, Japan*
[b] *Faculty of Engineering, Yokohama National University, Hodogaya-ku, Yokohama 240-8501, Japan*
[c] *Japan Biological Informatics Consortium, Chuo-ku, Tokyo 104-0032, Japan*
[d] *Jet Propulsion Laboratory, California Institute of Technology, Pasadena, CA 91109, USA*
[e] *Department of Biochemistry and Molecular Biophysics, University of Arizona, Tucson, AZ 85721, USA*
[f] *Institute for Molecular Science, Okazaki National Institutes, Myodaiji, Okazaki 444-8585, Japan*

Received 2 October 2002; revised 4 November 2002; accepted 5 November 2002

First published online 19 November 2002

Edited by Stuart Ferguson

Abstract **The macroscopic and microscopic redox potentials of the four hemes of the small tetraheme cytochrome *c* from *Shewanella oneidensis* were determined. The microscopic redox potentials show that the order of reduction is from hemes in the C-terminal domain (hemes 3 and 4) to the N-terminal domain (heme 1), demonstrating the polarization of the tetraheme chain during reduction. This makes heme 4 the most efficient electron delivery site. Furthermore, multi-step reduction of other redox centers through either heme 4 or heme 3 is shown to be possible. This has provided new insights into the two-electron reduction of the flavin in the homologous flavocytochrome *c*–fumarate reductase.**

Key words: Redox potential; Tetraheme cytochrome; Heme architecture; Cooperativity; NMR; Polarography

1. Introduction

Shewanella is a gram-negative facultative anaerobe able to grow under a variety of conditions [1]. *Shewanella oneidensis* (previously called *S. putrefaciens*) strain MR1 was specifically isolated as a metal oxide-reducing organism that could couple the reduction of metal oxides to the oxidation of organic carbon. Cytochromes have been implicated in this process and are abundant in *Shewanella* species [2]. The genome sequence analysis [3] indicates that *Shewanella oneidensis* (*So*) has more *c*-type cytochromes than any other species examined to date. Among them, soluble fumarate reductase (SFR, also called flavocytochrome *c*) and small tetraheme cytochrome *c* (STC) are relatively well characterized [4–13]. STC from *So* MR1 contains 91 amino acid residues, showing 34% identity with the cytochrome domain of SFR [11]. The crystal structures of SFR from both *Shewanella frigidimarina* (*Sf*) [6,7] and *So* [8], as well as the structures of *So* [13] and *Sf* STC [12], establish that the structure of the cytochrome domain of SFR is similar to that of STC. The architectures of the four hemes in STC and SFR are significantly different from that of cytochrome c_3 (cyt c_3) from the genus *Desulfovibrio* (Fig. 1). The chain-like heme architecture (Fig. 1B) is a characteristic feature of STC in contrast to the cyclic heme architecture in cyt c_3, where all four hemes are in contact. The significance of the multi-heme architecture is one of the major interests in the investigations of the *c*-type cytochromes [14].

We have characterized the redox properties of STC, and analyzed the results in terms of heme architecture. For the first time, the important role of the heme architecture in a multi-heme protein is apparent, with the reduction mechanism in STC providing new insights into the two-electron reduction of the flavin in SFR.

2. Materials and methods

So MR1 was cultured aerobically in a 50-l fermenter (Iwashiya) using LB medium. STC was purified according to the reported method with modifications [5]. Purity was confirmed by SDS–PAGE. Differential pulse polarograms were measured at dropping mercury electrodes with a potentiostat, Fuso Polarograph Model 312. The sample was dissolved in 300 mM KCl, 30 mM borate buffer (pH 9.0) at 0.4 mM protein concentration. The polarograms were fitted using the analytical equation for four consecutive one-electron reversible electrode reactions to obtain macroscopic redox potentials [15]. NMR spectra were recorded at 303 K on Bruker DRX400 and DRX600 NMR spectrometers with the samples at about 1 mM in deuterated 30 mM borate buffer (pH 8.7 and 9.1) without and with 300 mM KCl. The sample was reduced by adding aliquots of 1 M sodium dithionite. After the NMR measurement, pH was measured and used without correction for the isotope effect. 2D NOESY (mixing time, 100, 200 and 400 ms) and TOCSY (mixing time, 60 ms) spectra were measured to assign heme signals in the fully reduced state. NOESY (chemical exchange) spectra with a mixing time of 15 ms were used to assign the heme methyl signals in the intermediate oxidation states.

*Corresponding author. Fax: (81)-6-6879 8599.
E-mail address: akutsu@protein.osaka-u.ac.jp (H. Akutsu).

Abbreviations: STC, small tetraheme cytochrome *c*; SFR, soluble fumarate reductase; *So*, *Shewanella oneidensis*; *Sf*, *Shewanella frigidimarina*; S_i, i-electron reduced state; FAD, flavin adenine dinucleotide

PII: S0014-5793(02)03696-7

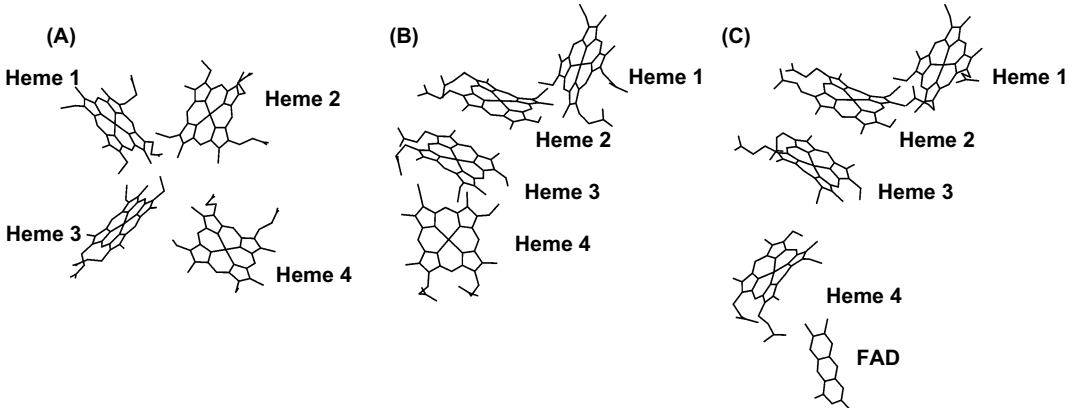

Fig. 1. Tetraheme architectures in small tetraheme cytochrome *c* from *Shewanella oneidensis* (B) [13], cytochrome c_3 from *Desulfovibrio vulgaris* Miyazaki F (A) [20] and soluble fumarate reductase from *Shewanella oneidensis* (C, with the flavin) [8].

3. Results and discussion

Differential pulse polarograms of *So* STC could not be obtained at low ionic strength, presumably because of denaturation of the protein at the electrode surface. Therefore, polarograms were recorded in the presence of 300 mM KCl at pH 9.0. The macroscopic redox potentials of *So* STC are −138, −192, −219 and −248 mV, which are substantially higher than those of cyt c_3 (for example, −234, −300, −330 and −368 mV at pH 9.0 [16]).

NMR spectra were obtained at pH 8.7 and 9.1, since the signals showed pH dependence in the neutral pH region. The effect of 300 mM KCl was small. All heme methyl and meso proton signals, and thioether methyl and methine proton signals in the fully reduced state were assigned for two pH values (Table 1 for pH 9.1). To avoid signal overlap, heme meso and thioether methine protons (7.22–9.79 and 5.18–6.61 ppm, respectively) were used for heme assignments. On the basis of the crystal structure of *So* STC in the reduced form [13], the pairs H4-5CH/H3-8^{2}CH$_3$ (3.52 Å), H3-20CH/H2-20CH (3.96 Å), H3-2^{1}CH$_3$/H2-20CH (4.32 Å), H3-20CH/H2-18^{1}CH$_3$ (4.13 Å), H2-5CH/H1-8^{2}CH$_3$ (3.81 Å), and H2-3^{2}CH$_3$/H1-8^{2}CH$_3$ (3.89 Å), where H4 refers to heme 4 (according to sequential numbering) and so on, with the carbon–carbon distances given in parentheses, are expected to give NOE cross peaks. In fact, these cross peaks were identified in the 2D NOESY spectra of the fully reduced protein, with the assignments of the cross peaks establishing that the groups a, b, c and d in Table 1 correspond to hemes 1, 3, 2 and 4, respectively. This heme assignment is consistent with that of *Sf* STC [12].

Fig. 2 shows portions of the NMR spectra of *So* STC at different stages of reduction. It is clear, by following the cross peaks, that five stages of heme methyl signals reflect the spectra of the five macroscopic oxidation states, S_0, S_1, S_2, S_3 and S_4 [11,16]. Here, subscripts 0, 1, 2, 3 and 4 stand for the fully oxidized state, and one-electron, two-electron, three-electron and fully reduced states, respectively. The ability to observe the individual macroscopic states means that the intramolecular and intermolecular electron exchange rates are much faster than 10^4 s^{-1} and slower than 10^2 s^{-1}, respectively. Table 2 summarizes the chemical shifts of the heme methyl signals in the five macroscopic oxidation states determined from cross peaks at pH 9.1. They are grouped based on the reduction fraction of each signal. Twelve out of 16 heme methyl signals could be assigned in all macroscopic oxidation states. The heme assignments given in the first column of Table 2 were determined by comparing the chemical shifts in the fully reduced state with those in Table 1. The reduction fraction of each heme was calculated using the chemical shifts for 18^{1}CH$_3$ of heme 1, 12^{1}CH$_3$ of heme 3 and 18^{1}CH$_3$ of heme 4 because they are positioned to the outside of the protein,

Table 1
Chemical shifts (ppm) of the heme protons of *So* ferroSTC at pH 9.1 and 303 K with 300 mM KCl

Heme proton	Heme groups			
	a (heme 1)	b (heme 3)	c (heme 2)	d (heme 4)
5 CH	8.99	9.08	9.61	9.85
10 CH	8.83	8.50	9.39	9.59
15 CH	9.53	9.79	9.75	9.41
20 CH	9.32	7.22	7.61	9.26
2^1 CH$_3$	3.64	1.89	2.69	3.46
7^1 CH$_3$	3.02	2.71	3.68	3.96
12^1 CH$_3$	3.50	3.57	3.47	3.51
18^1 CH$_3$	3.19	1.64	0.93	3.28
3^1 CH	5.66	5.79	6.61	5.98
8^1 CH	5.76	5.18	6.37	6.50
3^2 CH$_3$	2.09	1.90	2.84	2.73
8^2 CH$_3$	−0.21	−1.22	2.49	2.51

Table 2
Chemical shifts (ppm) of the heme methyl signals in the five macroscopic oxidation states of *So* STC at pH 9.1 and 303 K with 300 mM KCl

Heme number and signal	Chemical shift				
	S_0	S_1	S_2	S_3	S_4
Heme 1					
18^1 CH$_3$ (B)	35.49	35.09	33.04	20.25	3.17
7^1 CH$_3$	23.07	22.56	20.91	13.67	3.02
Heme 2					
18^1 CH$_3$	22.55	18.38	12.26	6.84	0.93
12^1 CH$_3$ (G)	21.27	18.96	12.84	9.03	3.46
7^1 CH$_3$	14.42	12.37	8.74	6.65	3.68
2^1 CH$_3$	13.36	11.41	7.82	5.70	2.69
Heme 3					
18^1 CH$_3$ (A)	38.87	22.52	18.49	7.42	1.63
12^1 CH$_3$	19.37	11.12	10.39	5.51	3.57
2^1 CH$_3$	17.13	10.64	8.74	4.27	1.89
7^1 CH$_3$	10.50	7.13	5.44	3.39	2.69
Heme 4					
18^1 CH$_3$ (C)	30.22	19.77	5.95	3.71	3.28
7^1 CH$_3$	26.95	18.63	5.88	4.12	3.96

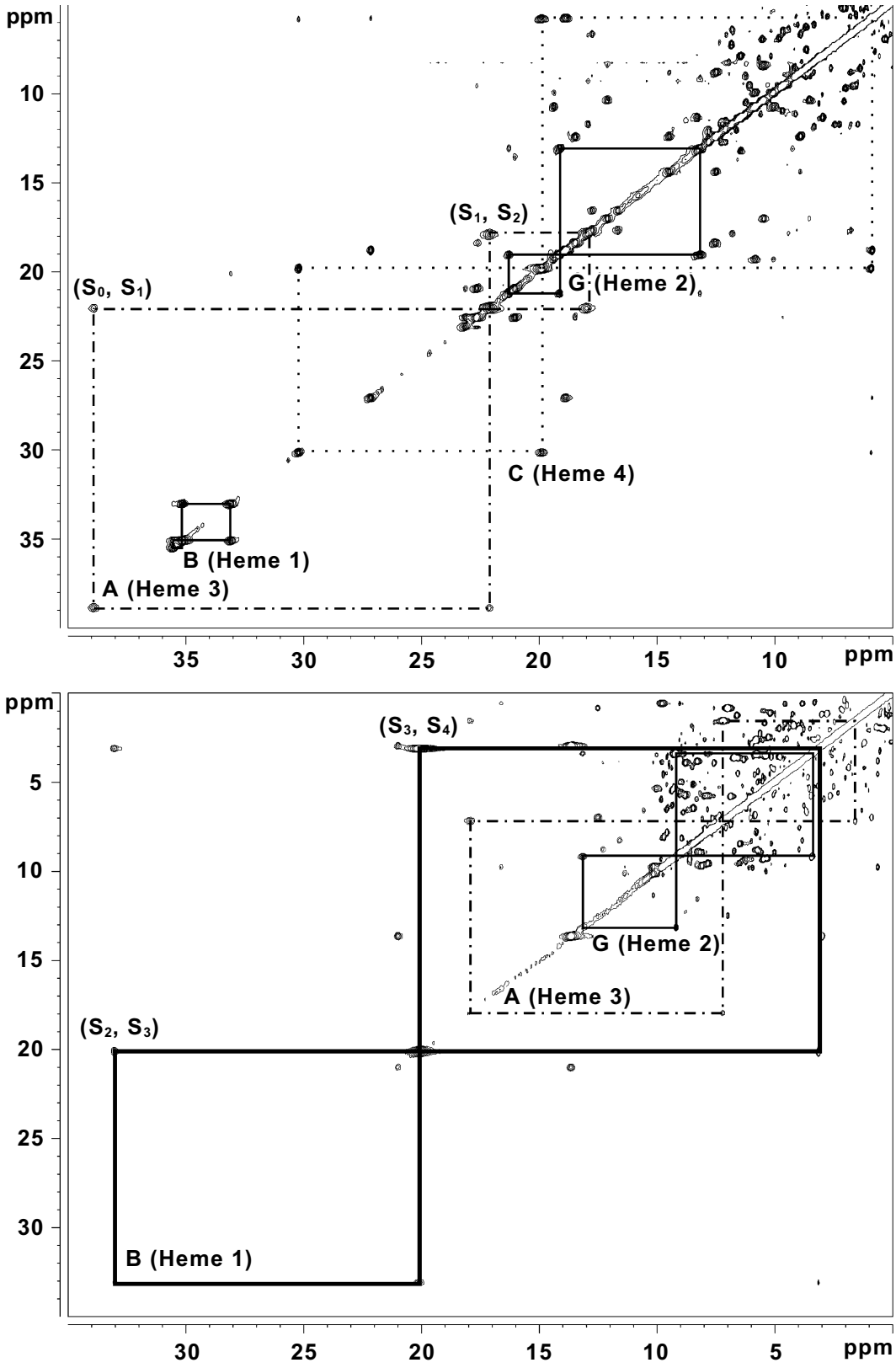

Fig. 2. Parts of the 2D chemical exchange NMR spectra of *So* STC in intermediate redox stages at pH 8.7. Top, coexistence of S_0, S_1 and S_2; bottom, coexistence of S_2, S_3 and S_4. A (dashed line), B (bold line), C (dotted line) and G (solid line) are heme methyl signals indicated in Table 2.

Table 3
Reduction fractions of the four hemes at the four reduction steps at pH 9.1 and 303 K with 300 mM KCl

	R^{I}	R^{II}	R^{III}	R^{IV}
Heme 1	0.006	0.068	0.395	0.531
Heme 2	0.110	0.356	0.214	0.320
Heme 3	0.503	0.059	0.308	0.130
Heme 4	0.381	0.517	0.083	0.019

The fraction of heme reduced at the i-th reduction step was calculated as $R^{i} = (\nu(S_{i-1}) - \nu(S_i))/(\nu(S_0) - \nu(S_4))$, where $\nu(S_i)$ is the chemical shift of a heme methyl signal in an i-electron reduced state (S_i).

hence, less likely to be influenced by adjacent chemical groups. There is no exposed heme methyl group for heme 2. Therefore, we selected $12^{1}CH_3$ for calculation, because it is not involved in stacking with heme 3. To correct for errors, the average reduction fractions were obtained by non-linear least squares fitting to $\Sigma_i R_i^j = \Sigma_j R_i^j = 1$ and given in Table 3 for pH 9.1.

As can be seen in Table 3, heme 3 is the principal heme reduced at the first reduction step, followed by heme 4 at the second step. Heme 1 is the principal heme reduced in both the third and fourth steps. The behaviors of hemes 1 and 4 are quite different from those reported for *Sf* STC. The reduction order in the latter was reported as hemes 3, 1, 2 and 4 [12]. This is in contrast to the similar chemical shifts of the heme proton signals in the fully reduced state of STC from both species. Examination of the STC heme methyl chemical shifts showed that their behavior on reduction is similar for the two species, although they were measured at different pH values. Only the chemical shifts of the 18^{1} methyl signals of hemes 1 and 4 are different, which leads to the different heme assignments. This complication originates from their similar chemical shift values (Table 2). To make this point clear, we assigned one additional signal for each heme, which confirmed our assignments. Microscopic redox potentials of the four hemes were calculated using the reduction fractions in Table 3 and macroscopic redox potentials [16]. The microscopic redox potentials for the first reduction step (e^{I}) are −272, −195, −155 and −163 mV, and those at the fourth step (e^{IV}) are −231, −218, −194 and −143 mV for hemes 1, 2, 3 and 4, respectively. The interacting potentials were $I_{12} = -3$, $I_{13} = 14$, $I_{14} = 30$, $I_{23} = -31$, $I_{24} = 12$ and $I_{34} = -22$ mV. Here, the subscripts refer to the heme number. Negative interacting potentials for direct neighbors and positive interacting potentials for other pairs are the characteristic features of the STC tetraheme chain.

It was suggested from the crystal structure that STC harvests electrons through all four hemes [13]. Here, we discuss the capability of each heme to supply an electron to another molecule based on the newly obtained results. Since the essential features of the redox potentials of STC at pH 7.0 are similar to those at pH 9.1 (data not shown), we can discuss the physiological significance of these features. The microscopic redox potentials of each heme at four reduction steps and the reduced fraction of each heme after reduction are presented in Fig. 3. The ordinate represents the energy. There are three bars in the central panels because of three redox molecular species for each heme (see legend). On addition of the first electron (S_1), the reduction fraction of heme 3 is the greatest. In S_2, heme 4 is the most reduced (about 90%), while heme 1 remains almost completely oxidized. This can be characterized as the polarization of the tetraheme chain. Taking the low solvent exposure of heme 3 into account, heme 4 should be the most efficient electron delivery site. The redox potential pattern changes in the third and fourth reduction steps. At this point, any heme can be used for supplying electrons to an electron acceptor. From the standpoint of driving force, heme 1 should be the most efficient site in S_3 and S_4. However, heme 4 remains central for multi-electron reduction because it is fully reduced in S_2, S_3 and S_4. Since I_{34} is negative, a cooperative two-electron reduction would be promoted. Namely, the redox potential of heme 4 with an electron at heme 3 is always the lowest (highest energy) in e_4 (e_4^{II3} and e_4 ^{III13} in Fig. 3II,III), thus providing more driving force for the oxidation of heme 4. Moreover, since heme 3 is reduced, the electron moves to heme 4 when the latter is oxidized, thus facilitating a cooperative two-electron reduction by the concerted electron transfer. From the thermodynamic point of view, hemes 4 and 3 should be considered as a

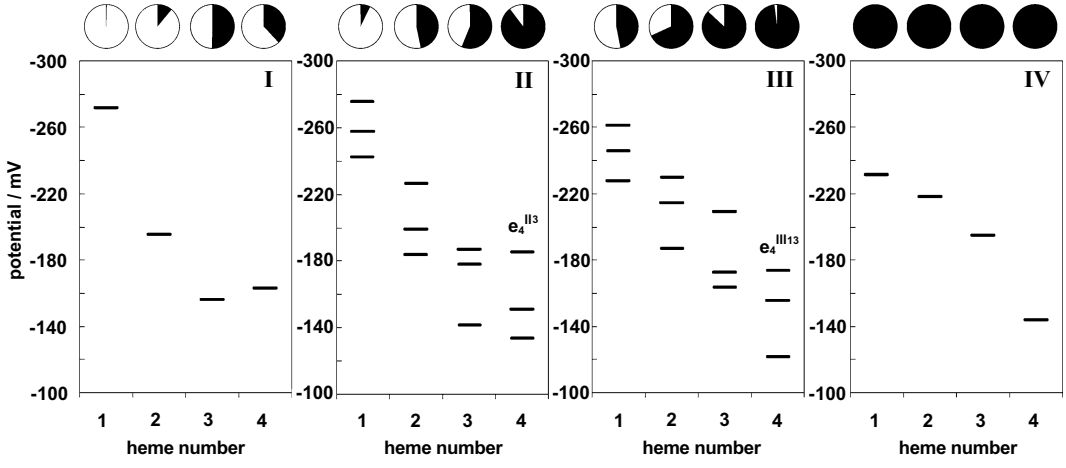

Fig. 3. Microscopic redox potentials and reduction fractions of four hemes of *So* STC at pH 9.1 with 300 mM KCl. Microscopic redox potentials are indicated for each heme. I, II, III and IV represent the reduction steps. The symbol e_4^{III13}, for example, stands for the microscopic redox potential of heme 4 at the third reduction step with hemes 1 and 3 already reduced. Since e_4^{III12} and e_4^{II23} are also possible, there are three lines in the column of heme 4. The presence of three lines for each heme in the two central panels is due to the same reason. The reduction fraction of each heme after the relevant reduction step (in S_1, S_2, S_3 and S_4, respectively) is presented on the top as a dark area in a circle.

kind of cooperative unit. Heme 3 is also a potential multi-electron delivery site, because the electron occupancy is more than 50% in S_1, S_2, S_3 and S_4. In this regard, flavocytochrome *c* provides some insights, since the tertiary structures of the SFR cytochrome domain and STC are similar and in SFR the flavin is oriented relative to hemes (Fig. 1C), presumably to optimize electron transfer.

In the crystal structures of *So* and *Sf* SFR, heme 4 is the site which makes contact with the target redox center, flavin [6–8]. This is consistent with our conclusion on the efficiency of heme 4. The two-electron redox potential of the flavin is about −152 mV, and the macroscopic redox potentials of the tetraheme chain are −102, −146, −196, and −238 mV [9]. Thus, the redox potential of the flavin is close to the second highest macroscopic potential of the heme chain, although the former is lower than the latter. This fact suggests that S_2, S_3 and S_4 oxidation states might be responsible for the reduction of the flavin. The flavin is reduced by a cooperative two-step reduction mechanism [9,17,18]. From the analysis of the electrochemical data, it was estimated that the electron transfer rate constant from the heme chain to flavin adenine dinucleotide (FAD; $\sim 100\ s^{-1}$) is slower than that among the hemes ($\sim 500\ s^{-1}$) [18]. The latter obtained by NMR was $> 10^4\ s^{-1}$ for STC. Therefore, equilibrium in the heme domain will be achieved prior to the electron transfer from a heme to FAD. Now the flavin reduction can be explained by our proposal for cooperative two-electron reduction by STC, involving hemes 4 and 3. Since we do not know the microscopic redox potentials of SFR heme 4 in S_2, we cannot eliminate the possibility that e_4^{II3} is lower than the redox potential of the first reduction of the flavin, which should be lower than −152 mV. It can be safely mentioned that the flavin can be reduced cooperatively by hemes 4 and 3 in S_3, since the thermodynamic driving force is enhanced by the presence of the third electron at heme 2 because of a significantly negative interacting potential between hemes 2 and 3 (I_{23}).

It is known that dried films of cyt c_3 are electrically conductive in S_4 [19]. This can be ascribed to the cyclic arrangement of the four hemes in cyt c_3, which act as an electron reservoir and can supply electrons in any direction depending on voltage. In the case of STC, there is a hierarchy in the redox potential along the tetraheme chain in S_4 (Fig. 3). Electrons entering at any heme would move to heme 4 along the downhill energy gradient. If there is a constant flow of electrons, the tetraheme chain should function as a directional electron conductive device in S_4 as a consequence of the heme architecture (Fig. 3). Given the importance of porphyrins and related molecules in nanotechnology, the heme architecture and properties of STC may provide some useful insights for the design of bioelectronic devices.

Acknowledgements: This work was partly supported by the Grant-in-Aid for Scientific Research from the Ministry of Education, Culture, Sports, Science and Technology of Japan and a grant from New Energy and Industrial Technology Development Organization to H.A. This work was also supported by grant GM21277 from the NIH to M.A.C.

References

[1] Nealson, K.H. and Saffarini, D.A. (1994) Annu. Rev. Microbiol. 48, 311–343.
[2] Myers, C.R. and Myers, J.M. (1997) Biochim. Biophys. Acta 1326, 307–318.
[3] Heidelberg, J.F. et al. (43 authors) (2002) Nat. Biotechnol. 20, 1118-1123.
[4] Pealing, S.L., Cheesman, M.R., Reid, G.A., Thomson, A.J., Ward, F.B. and Chapman, S.K. (1995) Biochemistry 34, 6153–6158.
[5] Tsapin, A.I., Nealson, K.H., Meyer, T.E., Cusanovich, M.A., Van Beeumen, J.J., Crosby, L.D., Feinberg, B.A. and Zhang, C. (1996) J. Bacteriol. 178, 6386–6388.
[6] Bamford, V., Dobbin, P.S., Richardson, D.J. and Hemmings, A.M. (1999) Nat. Struct. Biol. 6, 1104–1107.
[7] Taylor, P., Pealing, S.L., Reid, G.A., Chapman, S.K. and Walkinshaw, M.D. (1999) Nat. Struct. Biol. 6, 1109–1112.
[8] Leys, D., Tsapin, A.I., Nealson, K.H., Meyer, T.E., Cusanovich, M.A. and Van Beeumen, J.J. (1999) Nat. Struct. Biol. 6, 1113–1117.
[9] Turner, K.L., Doherty, M.K., Heering, H.A., Armstrong, F.A., Reid, G.A. and Chapman, S.K. (1999) Biochemistry 38, 3302–3309.
[10] Gordon, E.H.J., Pike, A.D., Hill, A.E., Cuthbertson, P.M. and Chapman, S.K. (2000) Biochem. J. 349, 153–158.
[11] Tsapin, A.I., Vandenberghe, I., Nealson, K.H., Scott, J.H., Meyer, T.E., Cusanovich, M.A., Harada, E., Kaizu, T., Akutsu, H., Leys, D. and Van Beeumen, J.J. (2001) Appl. Environ. Microbiol. 67, 3236–3244.
[12] Pessanha, M., Brennan, L., Xavier, A.V., Cuthbertson, P.M., Reid, G.A., Chapman, S.K., Turner, D.L. and Salguerio, C.A. (2001) FEBS Lett. 489, 8–13.
[13] Leys, D., Meyer, T.E., Tsapin, A.S., Nealson, K.H., Cusanovich, M.A. and Van Beeumen, J.J. (2002) J. Biol. Chem. 277, 35703–35711.
[14] Barker, P.D. and Ferguson, S.J. (1999) Structure 7, R281–R290.
[15] Niki, K., Kobayashi, Y. and Matsuda, H. (1984) J. Electroanal. Chem. 178, 333–341.
[16] Park, J.-S., Ohmura, T., Kano, K., Sagara, T., Niki, K., Kyogoku, Y. and Akutsu, H. (1996) Biochim. Biophys. Acta 1293, 45–54.
[17] Butt, J.N., Thornton, J., Richardson, D.J. and Dobbin, P.S. (2000) Biophys. J. 78, 994–1009.
[18] Jeuken, L.J.C., Jones, A.K., Chapman, S.K., Cecchini, G. and Armstrong, F.A. (2002) J. Am. Chem. Soc. 124, 5702–5713.
[19] Kimura, K., Nakahara, Y., Yagi, T. and Inokuchi, H. (1979) J. Chem. Phys. 70, 3317–3323.
[20] Harada, E., Fukuoka, Y., Ohmura, T., Fukunishi, A., Kawai, G., Fujiwara, T. and Akutsu, H. (2002) J. Mol. Biol. 319, 767–778.